APL Photonics

RESEARCH ARTICLE | OCTOBER 02 2019

Michelson interferometer modulator based on hybrid silicon and lithium niobate platform

Special Collection: Hybrid Integration beyond Silicon Photonics

Mengyue Xu; Wenjun Chen; Mingbo He; Xueqin Wen; Ziliang Ruan; Jian Xu; Lifeng Chen; Liu Liu; Siyuan Yu; Xinlun Cai

APL Photonics 4, 100802 (2019)
https://doi.org/10.1063/1.5115136

Michelson interferometer modulator based on hybrid silicon and lithium niobate platform

Cite as: APL Photon. 4, 100802 (2019); doi: 10.1063/1.5115136
Submitted: 15 June 2019 • Accepted: 5 September 2019 •
Published Online: 2 October 2019

Mengyue Xu,[1] Wenjun Chen,[1] Mingbo He,[1] Xueqin Wen,[2] Ziliang Ruan,[2] Jian Xu,[3] Lifeng Chen,[1,a)] Liu Liu,[2,b)] Siyuan Yu,[1] and Xinlun Cai[1,c)]

AFFILIATIONS

[1]State Key Laboratory of Optoelectronic Materials and Technologies and School of Electronics and Information Technology, Sun Yat-sen University, Guangzhou 510000, China
[2]South China Academy of Advanced Optoelectronics, South China Normal University, Guangzhou 510000, China
[3]School of Economics and Commerce, South China University of Technology, Guangzhou 510000, China

Note: This article is part of the Special Topic on Hybrid Integration beyond Silicon Photonics.
[a)]**Electronic mail:** chenlf37@mail.sysu.edu.cn
[b)]**Electronic mail:** liu.liu@coer-scnu.org
[c)]**Electronic mail:** caixlun5@mail.sysu.edu.cn

ABSTRACT

We propose and demonstrate a hybrid silicon and lithium niobate Michelson interferometer modulator (MIM) with a reduced half-wave voltage-length product compared to a Mach-Zehnder modulator. The modulator is based on seamless integration of a high-contrast waveguide based on lithium niobate—a widely used modulator material—with compact, low-loss silicon circuitry. The present device demonstrates a half-wave voltage-length product as low as 1.2 V cm and a low insertion loss of 3.3 dB. The 3 dB electro-optic bandwidth is approximately 17.5 GHz. The high-speed modulations are demonstrated at 32 Gbit/s and 40 Gbit/s with the extinction ratio of 8 dB and 6.6 dB, respectively. The present device avoids absorption loss and nonlinearity in conventional silicon modulators and demonstrates the lowest half-wave voltage-length product in lithium niobate modulators. The hybrid MIM demonstrates high-speed data modulation showing potential in future optical interconnects.

I. INTRODUCTION

Silicon photonics on the silicon-on-insulator (SOI) platform has emerged as the leading technology for optical interconnect due to the possibility of low-cost and high-volume production of photonic integrated circuits (PICs) in CMOS foundries.[1–3] However, optical modulations in the silicon material mainly rely on free-carrier plasma dispersion effect, which leads to inevitable absorption losses, nonlinear voltage response, and temperature sensitivity.[4,5] Lithium niobate ($LiNbO_3$, LN) shows potential for realizing high performance electro-optic (EO) modulators due to its physical properties: large EO coefficient (30 pm/V), strong Pockels effect, wide bandgap (wide transparency window), and good temperature stability.[6] Nevertheless, commercial bulk LN modulators based on the indiffused or proton-exchange waveguide are suffering with a low refractive index contrast, large half-wave voltage-length product ($V_\pi \cdot L$, typically >10 V cm),[7] and difficult to integrate.

Lithium niobate on insulator (LNOI) has been reported as a promising platform for photonic integrated devices.[7–11] A typical cross section of a LNOI photonic waveguide is less than 1 μm^2, which leads to a small mode size and tight mode confinement. As a result, the LNOI-based modulator allows for a good overlap between optical and electrical fields and reduced $V_\pi \cdot L$. Recently, the integrated LN modulator has shown low loss, low drive voltage, and large bandwidth.[12] An alternative approach, i.e., heterogeneous integration of LN membranes onto SOI photonic integrated circuits, has also attracted considerable interest.[13–18] The silicon/LN material system combines the scalability of silicon photonics with excellent modulation performance of LN. More recently, by etching the LN membrane, we have demonstrated a Mach-Zehnder modulator

(MZM) based on the heterogeneous silicon/LN platform with low loss and large modulation bandwidth.[19]

In this letter, we propose and demonstrate a Michelson interferometer modulator (MIM) based on the heterogeneous silicon/LN platform [Fig. 1(a)]. In contrast with the traveling wave MZM structures, light wave is reflected by the reflective mirrors at the end of both arms, and the interaction length between the light wave and modulating electrical field doubles.[20–23] Figure 1(a) shows our heterogeneous silicon/LN MIM design. The MIM consists of a bottom silicon waveguide layer, a top LN waveguide layer, and vertical adiabatic couplers (VACs) which transfer the optical power between the two layers. The top LN waveguides, formed by dry-etching of an X-cut LN thin film, serve as phase modulators where EO interactions occur. The bottom SOI circuit supports all other passive functions, consisting of a 3 dB multimode interference (MMI) coupler that splits and combines the optical power, two loop mirrors that serve as broadband reflectors, and two grating couplers for off-chip coupling. The VACs, which were formed by silicon inverse tapers and superimposed LN waveguides, serve as interfaces to couple light up and down between the two layers. A mode calculation result [using finite difference eigenmode (FDE) solver, Lumerical Mode Solution[24]] indicates the optical mode transferring 99.9% energy from the modulation region (mode "A") to the beginning of VAC (mode "B"), and vice versa. The simulated result indicates the thickness of the benzocyclobutene (BCB) adhesive can be varied from 220 nm to 400 nm with negligible degradation in coupling efficiency. The continuous wave (CW) laser couples into the waveguide from one of the grating couplers. The RF signal is applied to ground-signal-ground (GSG) electrodes, and modulated light is detected at another grating coupler.

II. DEVICE DESIGN AND FABRICATION

The device fabrication process is shown in Fig. 1(b). First, silicon grating couplers, MMIs, waveguide loop mirrors, and inverse tapers are patterned by SOI processing including e-beam lithography (EBL) and dry etching. Then, a commercially available X-cut LN membrane on an insulator (600 nm thick LN film on 3 μm SiO_2) wafer from NanoLN is then flipped and bonded onto the patterned silicon wafer covered by 300 nm thick BCB. Removing the silicon substrate and oxide layer of the LNOI wafer leaves a stack of Si/BCB/LN/SiO_2 on the host substrate. Afterward, the top LN waveguides, serving as phase modulators where Pockels effect occur, are defined by e-beam lithography (EBL) writing on a hydrogen

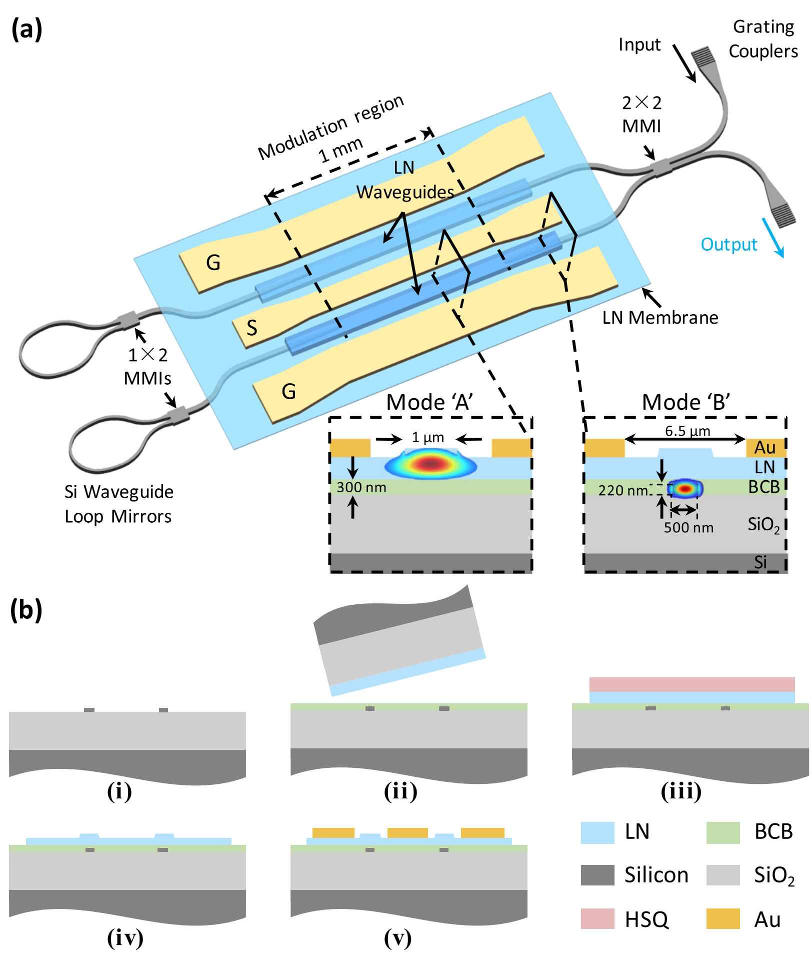

FIG. 1. (a) 3D schematic of a heterogeneous silicon/LN MIM, and insets are cross-sectional views of calculated optical TE0 mode in (mode "A") the modulation region and (mode "B") the beginning of VAC. (b) Device fabrication process.

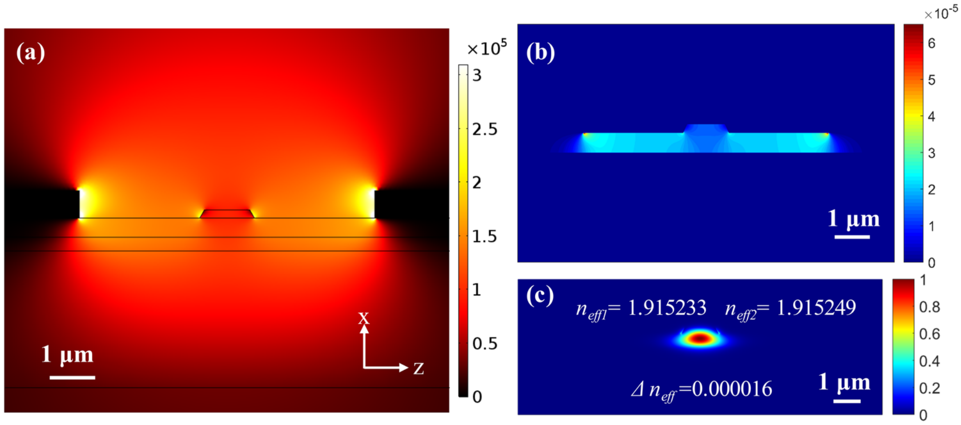

FIG. 2. Cross-sectional view (shown in E_z components) of the simulated (a) electric field distribution when a fixed voltage of 1 V is applied across the two electrodes, (b) refractive index change distribution, and (c) optical mode profile. The effective index of the TE_0 guided mode increased from n_{eff1} to n_{eff2} when the electric field is applied. Δn_{eff} is the change of the effective index.

silsesquioxane (HSQ) resist. The waveguide patterns are then transferred into the LN thin film using optimized argon plasma etching in an inductively coupled plasma (ICP) etching system. Finally, a pair of traveling-wave electrodes, configured in a ground–signal–ground form, is fabricated directly on the LN layer by a liftoff process. To achieve a large bandwidth, the GSG electrodes are simulated in ANSYS HFSS and optimized for 50 Ω impedance matching. The characteristic impedance (Z_c) of the electrodes varies between 56.3 Ω and 51.17 Ω from 2.5 GHz to 70 GHz. The thickness of the Au electrode is 600 nm, and the widths of signal and ground electrodes are 19.5 μm and 30 μm, respectively.

The design waveguides have a top width of 1 μm, a rib height of 180 nm, a slab thickness of 420 nm, and the electrode spacing of 6.5 μm. The aim of the design is to enable low $V_\pi \cdot L$ and low metal absorption loss. The cross-sectional view of the simulated electric field distribution (E_z) is shown in Fig. 2(a). The result

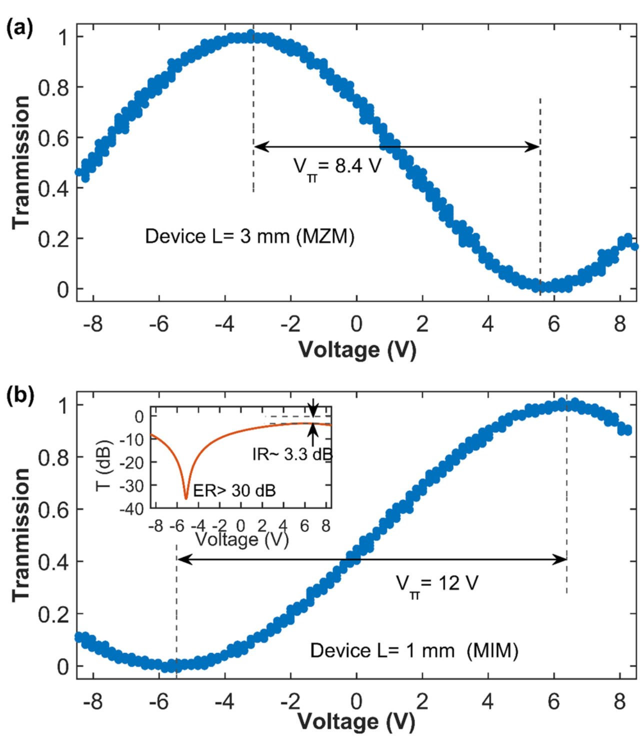

FIG. 3. Normalized optical transmission of (a) a 3-mm-long MZM and (b) a 1-mm-long MIM as a function of the applied voltage. The inset is the transmission normalized to input from grating couplers and shown in the log scale.

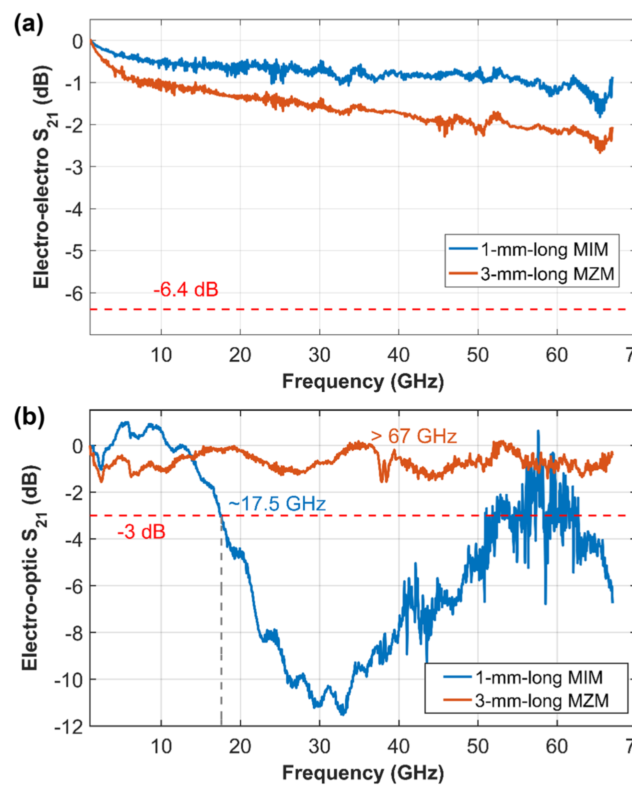

FIG. 4. The measured (a) electro-electro bandwidth (S_{21} parameter) and (b) electro-optic bandwidth (S_{21} parameter) of a 1-mm-long MIM (~17.5 GHz) and a 3-mm-long MZM (>67 GHz); dashed red lines indicate the 6.4 dB threshold of EE in (a) and 3 dB threshold of EO in (b). S_{21}, transmission coefficient of the scattering matrix.

is obtained from a commercial software (COMSOL Multiphysics[25]) when a fixed voltage of 1 V is applied cross the two electrodes. The EO refractive index change (Δn) distribution in the LN material is shown in Fig. 2(b). Assume that the optical wave propagates along the y-axis and the direction of the applied electrical field is along the z-axis on an X-cut LN wafer, the Δn in the LN waveguide with a fixed applied voltage of 1 V is calculated by

$$\Delta n = \frac{E_z n_e^3 r_{33}}{2}, \tag{1}$$

where n_e is the LN refractive index of 2.138 and r_{33} is the highest EO coefficient of LN of ~30 pm/V.[26] The Δn results in the change of the effective index of the TE_0 guided mode (Δn_{eff}) in the etched LN waveguide. Then, we use an optical FDE solver (Lumerical Mode Solution[24]) to solve the n_{eff} for the fundamental TE mode without and with the electric field [shown in Figs. 2(c) and 2(d)]. The Δn_{eff} of our design is 0.000 016 when the applied voltage is 1 V. The single arm phase change of MIM in the push-pull configuration is calculated by

$$\Delta\varphi = \frac{V}{V_\pi}\frac{\pi}{2} = \Delta\beta L = \frac{2\pi}{\lambda_0}\Delta n_{eff} L, \tag{2}$$

where V is the fixed applied voltage of 1 V, L is the physical modulation length, $\Delta\beta$ is the change of the propagation constant, and λ_0 is the operating wavelength of 1550 nm. Therefore, we can calculate the value of $V_\pi \cdot L$ through solving Δn_{eff} for TE_0 mode at a wavelength of 1550 nm. Our design has a calculated $V_\pi \cdot L$ of ~1.2 V cm and a total loss of 0.3 dB/cm.

III. DEVICE CHARACTERIZATION

To compare the performance of modulation efficiency and modulation bandwidth between MZM and MIM, we adopt the above-mentioned design and fabrication process for a 1-mm-long MIM and a 3-mm-long MZM, both in a push-pull configuration. First, we performed half of wave voltage (V_π) measurements with a 100-kHz triangular voltage sweep[18] for both modulators to evaluate modulation efficiency. Note that all measurements used 1550 nm wavelength as the source center wavelength. The measured V_π of a 3-mm-long MZM is 8.4 V [shown in Fig. 3(a)], corresponding to $V_\pi \cdot L$ of 2.52 V cm. Figure 3(b) shows that the V_π measured from the 1 mm-long MIM device is 12 V, corresponding to $V_\pi \cdot L$ of 1.2 V cm that is lower than half of $V_\pi \cdot L$ in the 3 mm-long MZM. This indicates that the MIM has half of $V_\pi \cdot L$ compared to the MZM as expected. The inset of Fig. 3(b) is the log-scaled transmission as a function of applied voltage, which shows the DC extinction ratio (ER) of >30 dB and the insertion loss of ~3.3 dB for the 1 mm MIM device. The total fiber-to-fiber loss is measured as 12.4 dB, including the coupling loss for per grating coupler (~4.7 dB) and 0.13 dB loss for per VAC. We believe that this $V_\pi \cdot L$ value of our MIM is the lowest amongst all previously reported thin-film LN devices.[12,13,15,16]

We then use a vector network analyzer (VNA, Agilent N5227A) to characterize the small signal EO bandwidth (S21 parameter) of our MIM and MZM devices. Losses of RF cables and microwave probes (GGB 67A) are subtracted by using short-open-load-thru (SOLT) calibration standard with calibration substrates (GGB CS-5). The optical modulated signal is preamplified by an erbium-doped

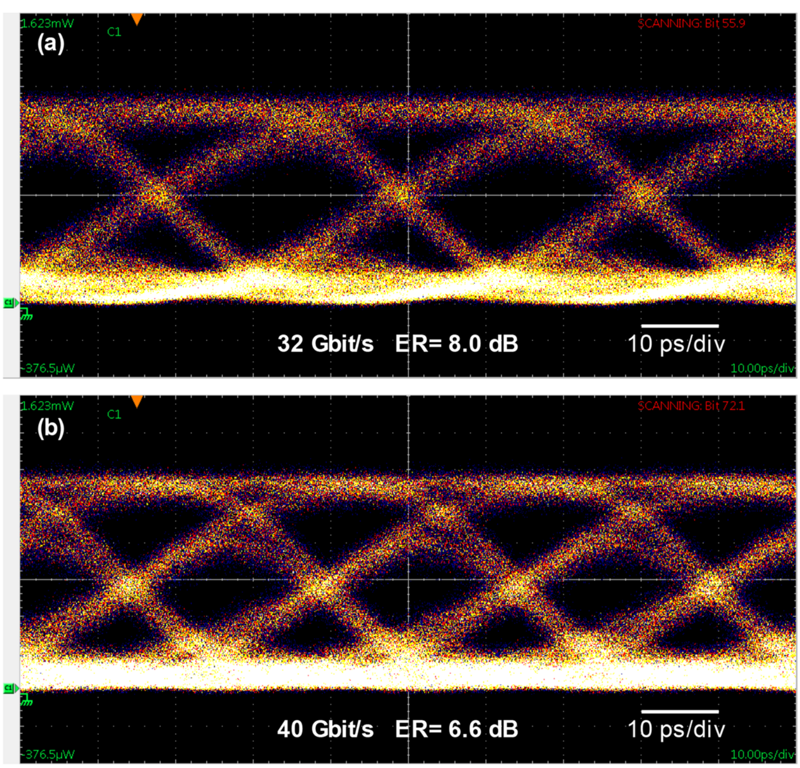

FIG. 5. The measured optical open eye diagrams at (a) 32 Gbit/s and (b) 40 Gbit/s under bias voltage lower than the quadrature point. The dynamic extinction ratios are 8.0 dB and 6.6 dB, respectively.

TABLE I. Comparison of several performance metrics for silicon MIMs. NA, not available.

References	Length of modulation area	$V_\pi \cdot L$	Insertion loss (dB)	EO bandwidth (GHz)	OOK data rate (Gbit/s)
21	500 μm	0.72–0.91	~8	NA	30
22	500 μm	0.72	7.6[a]	13.3[b]	40
23	1 mm	0.95–1.26	3	<10	20
This work	1 mm	1.2	3.3	17.5	40

[a]The value is calculated from 8.8 dB fiber-to-fiber loss and 1.2 dB routing loss from the grating couplers.
[b]The value is measured with a source impedance of 50 Ω alone.

fiber amplifier (EDFA, Amonics AEDFA-PKT-DWDM-15-8-FA) and detected by a 70 GHz EO bandwidth photodiode (PD, FINISAR XPDV3120R). The electrode termination is loaded with 50 Ω. The EO bandwidth of our modulators is obtained by deducting the known EO S_{21} of the PD. Figure 4 demonstrates the measurement result of electro-electro (EE) and electro-optic (EO) S_{21} parameter response as a function of the input frequency sweep in a 1-mm-long MIM (blue solid line) and a 3-mm-long MZM (red solid line). The measured EE S_{21} is well above −6.4 dB point until 67 GHz. This indicates low losses of RF signal in the transmission line for both modulators. The measured −3 dB EO bandwidth of MIM is about 17.5 GHz [see in Fig. 4(b)] when the modulator is biased at a quadrature point (~0.5 V). For a MZM with the same RF electrode design, it shows EO bandwidth above 67 GHz when it is biased at 1.6 V. Because of the same RF electrode design for MIM and MZM, both modulators have the same impedance and microwave attenuation coefficient for electrodes. Additionally, MZM having an ultra-high bandwidth indicates well electro-optical velocity match. The microwave signal propagates only one way along the transmission line from the launch pad to 50 Ω termination; however, the optical signal travels forward and backward along the waveguide due to the reflection of loop mirrors in MIM, which leads to electro-optical velocity mismatch.

To obtain the performance of our MIM in high-speed digital data transmission, we performed on-off keying (OOK) modulation measurements. Figure 5 shows non-return-to-zero (NRZ) open eye diagrams at 32 Gbit/s and 40 Gbit/s. A pseudorandom binary sequence (PRBS) of length 2^{11}-1 at 32 Gbit/s and 40 Gbit/s is obtained from an arbitrary waveform generation (AWG, Micram) and then amplified by a linear amplifier (SHF 807) with a peak-to-peak voltage (V_{pp}) of 6.1 V. Eye diagrams are obtained from a sampling oscilloscope (Tektronix 8300) without any electrical compensations. When the modulator is biased at 0.1 V lower than the quadrature point, we measured the dynamic ERs are 8 dB at 32 Gbit/s and 6.6 dB at 40 Gbit/s, as shown in Figs. 5(a) and 5(b), respectively. Our device operates at data rates higher than the measured 3 dB EO bandwidth because of the high electrical signal quality.

IV. CONCLUSION

In summary, we demonstrate a heterogeneous silicon and LN MIM in compact footprint (0.1 mm^2) with half of $V_\pi \cdot L$ compared to a MZM. The lowest $V_\pi \cdot L$ in the LN platform of 1.2 V cm is achieved. In the OOK eye diagram measurement, we have shown open optical eye diagram data rates up to 40 Gbit/s with 6.6 dB extinction ratio, which is comparative to that of silicon modulators. The present device demonstrates an appealing insertion loss of around 3 dB. In Table I, we compare the performance of the present device with silicon MIMs. The present device in this work is the only one in which low insertion loss and competitive performance of data modulation are demonstrated simultaneously. Moreover, this hybrid platform can also avoid some disadvantages in conventional silicon modulators, such as absorption loss and nonlinearity. It should be noted that the present MIM showed a limited EO bandwidth, which is because the velocity matching cannot be achieved for both propagation synchronously. The LNOI platform is a promising candidate for low-loss, low-voltage, and high-speed modulators; however, CMOS-compatible drive voltage can only be realized when the length of the device exceeds 1 cm in a Mach-Zehnder interferometer configuration.[12] MIM can be a choice if the requirement for the bandwidth is not that high but the demand of footprint is rigorous. Especially, in the scenario of short reach interconnect, the footprint is very important, and MIM can offer a choice for the low-loss and compact modulator.

ACKNOWLEDGMENTS

This work was supported by the National Natural Science Foundation of China (NSFC) under Grant Nos. 11690031, 61575224, and 61622510, the Key R&D Program of Guangdong Province (Grant No. 2018B030325002), the Local Innovative and Research Teams Project of Guangdong Pearl River Talents Program (Grant No. 2017BT01X121), Characteristic Innovation Projects of Universities in Guangdong Province (Grant No. 2017WTSCX002), Natural Science Foundation for Ph.D. in Guangdong Province (Grant No. B6180990), and International Cooperation Open Project of State Key Laboratory of Subtropical Building Science, South China University of Technology (Grant No. 2019ZA02).

REFERENCES

[1] W. Bogaerts, R. Baets, P. Dumon, V. Wiaux, S. Beckx, D. Taillaert, B. Luyssaert, J. V. Campenhout, P. Bienstman, and D. V. Thourhout, "Nanophotonic waveguides in silicon-on-insulator fabricated with CMOS technology," J. Lightwave Technol. **23**, 401 (2005).
[2] A. H. Atabaki, S. Moazeni, F. Pavanello, H. Gevorgyan, J. Notaros, L. Alloatti, M. T. Wade, C. Sun, S. A. Kruger, H. Meng, K. Al Qubaisi, I. Wang, B. Zhang,

A. Khilo, C. V. Baiocco, M. A. Popović, V. M. Stojanović, and R. J. Ram, "Integrating photonics with silicon nanoelectronics for the next generation of systems on a chip," Nature **556**, 349–354 (2018).
[3] G. T. Reed and A. P. Knights, *Silicon Photonics: An Introduction* (John Wiley & Sons, 2004).
[4] G. T. Reed, G. Mashanovich, F. Y. Gardes, and D. J. Thomson, "Silicon optical modulators," Nat. Photonics **4**, 518 (2010).
[5] Q. Xu, B. Schmidt, S. Pradhan, and M. Lipson, "Micrometre-scale silicon electro-optic modulator," Nature **435**, 325 (2005).
[6] E. L. Wooten, K. M. Kissa, A. Yi-Yan, E. J. Murphy, D. A. Lafaw, P. F. Hallemeier, D. Maack, D. V. Attanasio, D. J. Fritz, G. J. McBrien, and D. E. Bossi, "A review of lithium niobate modulators for fiber-optic communications systems," IEEE J. Sel. Top. Quantum Electron. **6**, 69–82 (2000).
[7] D. Janner, D. Tulli, M. Garcia-Granda, M. Belmonte, and V. Pruneri, "Micro-structured integrated electro-optic $LiNbO_3$ modulators," Laser Photonics Rev. **3**, 301–313 (2009).
[8] G. Poberaj, H. Hu, W. Sohler, and P. Günter, "Lithium niobate on insulator (LNOI) for micro-photonic devices," Laser Photonics Rev. **6**, 488–503 (2012).
[9] A. Boes, B. Corcoran, L. Chang, J. Bowers, and A. Mitchell, "Status and potential of lithium niobate on insulator (LNOI) for photonic integrated circuits," Laser Photonics Rev. **12**, 1700256 (2018).
[10] L. Chang, Y. F. Li, N. Volet, L. R. Wang, J. Peters, and J. E. Bowers, "Thin film wavelength converters for photonic integrated circuits," Optica **3**, 531–535 (2016).
[11] A. Rao and S. Fathpour, "Compact lithium niobate electrooptic modulators," IEEE J. Sel. Top. Quantum Electron. **24**, 1–14 (2018).
[12] C. Wang, M. Zhang, X. Chen, M. Bertrand, A. Shams-Ansari, S. Chandrasekhar, P. Winzer, and M. Lončar, "Integrated lithium niobate electro-optic modulators operating at CMOS-compatible voltages," Nature **562**, 101–104 (2018).
[13] P. O. Weigel, J. Zhao, K. Fang, H. Al-Rubaye, D. Trotter, D. Hood, J. Mudrick, C. Dallo, A. T. Pomerene, A. L. Starbuck, C. T. DeRose, A. L. Lentine, G. Rebeiz, and S. Mookherjea, "Bonded thin film lithium niobate modulator on a silicon photonics platform exceeding 100 GHz 3-dB electrical modulation bandwidth," Opt. Express **26**, 23728–23739 (2018).
[14] L. Chen, Q. Xu, M. G. Wood, and R. M. Reano, "Hybrid silicon and lithium niobate electro-optical ring modulator," Optica **1**, 112–118 (2014).
[15] A. J. Mercante, P. Yao, S. Y. Shi, G. Schneider, J. Murakowski, and D. W. Prather, "110 GHz CMOS compatible thin film $LiNbO_3$ modulator on silicon," Opt. Express **24**, 15590–15595 (2016).
[16] A. Rao, A. Patil, P. Rabiei, A. Honardoost, R. DeSalvo, A. Paolella, and S. Fathpour, "High-performance and linear thin-film lithium niobate Mach–Zehnder modulators on silicon up to 50 GHz," Opt. Lett. **41**, 5700–5703 (2016).
[17] P. O. Weigel, M. Savanier, C. T. DeRose, A. T. Pomerene, A. L. Starbuck, A. L. Lentine, V. Stenger, and S. Mookherjea, "Lightwave circuits in lithium niobate through hybrid waveguides with silicon photonics," Sci. Rep. **6**, 22301 (2016).
[18] P. Rabiei, J. Ma, S. Khan, J. Chiles, and S. Fathpour, "Heterogeneous lithium niobate photonics on silicon substrates," Opt. Express **21**, 25573–25581 (2013).
[19] M. He, M. Xu, Y. Ren, J. Jian, Z. Ruan, Y. Xu, S. Gao, S. Sun, X. Wen, L. Zhou, L. Liu, C. Guo, H. Chen, S. Yu, L. Liu, and X. Cai, "High-performance hybrid silicon and lithium niobate Mach–Zehnder modulators for 100 Gbit s^{-1} and beyond," Nat. Photonics **13**, 359–364 (2019).
[20] J. F. Song, Q. Fang, S. H. Tao, T. Y. Liow, M. B. Yu, G. Q. Lo, and D. L. Kwong, "Fast and low power Michelson interferometer thermo-optical switch on SOI," Opt. Express **16**, 15304–15311 (2008).
[21] X. Y. Li, X. Xiao, H. Xu, Z. Y. Li, T. Chu, J. Z. Yu, and Y. D. Yu, "Highly efficient silicon Michelson interferometer modulators," IEEE Photonics Technol. Lett. **25**, 407–409 (2013).
[22] D. Patel, V. Veerasubramanian, S. Ghosh, A. Samani, Q. H. Zhong, and D. V. Plant, "High-speed compact silicon photonic Michelson interferometric modulator," Opt. Express **22**, 26788 (2014).
[23] M. J. Wang, L. J. Zhou, H. K. Zhu, Y. Y. Zhou, Y. M. Zhong, and J. P. Chen, "Low-loss high-extinction-ratio single-drive push-pull silicon Michelson interferometric modulator," Chin. Opt. Lett. **15**, 042501 (2017).
[24] See https://www.lumerical.com for Lumerical Solutions, Inc.
[25] See www.comsol.com for COMSOL Multiphysics® version 5.4, COMSOL AB, Stockholm, Sweden.
[26] D. N. Nikogosyan, *Nonlinear Optical Crystals: A Complete Survey* (Springer Science & Business Media, 2006).